

Transfer Learning for Brain-Computer Interfaces: An Euclidean Space Data Alignment Approach

He He and Dongrui Wu, *Senior Member, IEEE*

Abstract—Almost all EEG-based brain-computer interfaces (BCIs) need some labeled subject-specific data to calibrate a new subject, as neural responses are different across subjects to even the same stimulus. So, a major challenge in developing high-performance and user-friendly BCIs is to cope with such individual differences so that the calibration can be reduced or even completely eliminated. This paper focuses on the latter. More specifically, we consider an offline application scenario, in which we have unlabeled EEG trials from a new subject, and would like to accurately label them by leveraging auxiliary labeled EEG trials from other subjects in the same task. To accommodate the individual differences, we propose a novel unsupervised approach to align the EEG trials from different subjects in the Euclidean space to make them more consistent. It has three desirable properties: 1) the aligned trial lie in the Euclidean space, which can be used by any Euclidean space signal processing and machine learning approach; 2) it can be computed very efficiently; and, 3) it does not need any labeled trials from the new subject. Experiments on motor imagery and event-related potentials demonstrated the effectiveness and efficiency of our approach.

Index Terms—Brain-computer interface, data alignment, EEG, Riemannian geometry, transfer learning

I. INTRODUCTION

A brain-computer interface (BCI) [15], [25] is a communication pathway for a user to interact with his/her surroundings by using brain signals, which contain information about the user's cognitive state or intentions. Electroencephalogram (EEG) is the most popular input in BCI systems. EEG-based BCIs mainly have three paradigms: steady-state visual evoked potentials (SSVEP), motor imagery (MI), and event-related potentials (ERPs). This paper focuses on the last two.

For MI-based BCIs, the user needs to imagine the movements of his/her body parts (e.g., hands, feet, and tongue), which causes rhythmic oscillations of the involved cortical areas. So, the imagination of different movements can be distinguished from the spatial localization of different sensorimotor rhythm modulations, and then used to control external devices. For ERP-based BCIs, the user is stimulated by a majority of common stimuli (non-target) and a small amount of rare stimuli (target). The EEG response shows a large positive peak in potential about 300ms (which is called a P300 signal) after the user perceives a target stimulus. So, a target stimulus can be detected by determining if there is a P300 signal associated with it.

Early BCI systems were mainly used to help people with disabilities [20]. For example, MI-based BCIs have been used to help severely paralyzed patients to control powered exoskeletons or wheelchairs without the involvement of muscles, and P300 spellers enable patients who can not move nor speak to type. Recently, the application scope of BCIs has been extended to normal people [18], [24], and EEG becomes the most popular input signal because it is easy and economic to acquire, safe (no surgery needed), and has high temporal resolution. However, EEG measures the very weak brain electrical signals from the scalp, which results in poor spatial resolution and low signal-to-noise ratio [4].

Consequently, sophisticated signal processing and machine learning algorithms are needed in EEG-based BCI systems to decode the EEG signal, especially for single-trial classification of EEG signals in real-world applications. Usually the EEG signals are first band-pass filtered and spatially filtered to increase the signal-to-noise ratio, and then discriminative features are extracted, which are next fed into machine learning algorithms such as Linear Discriminant Analysis (LDA) and Support Vector Machine (SVM) [3] for classification.

The covariance matrix of multi-channel EEG signals plays an important role in signal processing. For instance, common spatial pattern (CSP) filters [12], [14], [17], [21], computed directly from the covariance matrices, are the most popular spatial filters for MI. An intuitive explanation is that the interactions between different channels are encoded in the covariance matrices, which can be decomposed to find the spatial distribution of brain activities.

Recent years have also witnessed an increasing interest in using the EEG covariance matrices for both classification and regression [1], [7], [31], [32]. Since the covariance matrices are symmetric positive definite (SPD) and lie on a Riemannian manifold, a popular approach is to view each covariance matrix as a point in the Riemannian space, and use its geodesic to the Riemannian mean as a feature in classification. This approach is called the Minimum Distance to Riemannian Mean (MDRM) classifier [1], [7], [32].

Although these signal processing and machine learning algorithms have achieved promising performances given enough subject-specific calibration trials, it is still almost impossible to design a generic BCI system that suits all subjects because people show strong individual differences in neural responses to even the same stimulus. As a result, these algorithms need to be calibrated by using some labeled subject-specific data. This calibration session could be time-consuming and not user-friendly. So, it is crucial to reduce or even completely eliminate the calibration.

He He and Dongrui Wu are with the Key Laboratory of the Ministry of Education for Image Processing and Intelligent Control, School of Automation, Huazhong University of Science and Technology, Wuhan 430074, China. Email: hehe91@hust.edu.cn, drwu@hust.edu.cn.

Dongrui Wu is the corresponding author.

Transfer learning (TL) [19], which leverages auxiliary labeled data from related sessions and/or subjects to help the calibration for a new subject, is a promising solution to the above challenge [13], [26], [27], [29], [30]. Recently, Zanini et al. [33] proposed a TL framework for the MDRM classifier (referred as Riemannian alignment (RA)-MDRM in this paper). It assumes the covariance matrices of different EEG trials shift across sessions with respect to a reference state, and move over in the same direction when involving a specific task. Thus, the covariance matrices of EEG trials of each session or subject can be transformed and aligned using a reference state, which is estimated by the mean covariance matrix of the resting state. In MI, the resting state is the time window that the subject is not performing any task, e.g., the transition window between two successive imageries. In ERP, particularly the rapid serial visual presentation (RSVP), the stimuli are presented quickly one after another and the responses overlap, so it is difficult to find the resting state. [33] used the non-target stimuli as the resting state in ERP, which requires that some calibration trials from the new subject must be known.

Experiments have shown that RA-MDRM outperformed MDRM in MI and ERP tasks [33]. But as mentioned above, it still needs a small amount of labeled subject-specific calibration trials for ERP classification. Moreover, for both MI and ERP, the classification is performed in the Riemannian space, whose geodesic computation is much more complicated, time-consuming and unstable than the distance calculation in the Euclidean space. In this paper we propose a new EEG data alignment approach in the Euclidean space, which has the following desirable characteristics:

- 1) It transforms and aligns the EEG data in the Euclidean space, which may have broader applications because most signal processing and machine learning algorithms are proposed for the Euclidean space.
- 2) It can be computed several times faster than RA.
- 3) It only requires unlabeled EEG trials but does not need any label information from the new subject; so, it can be used in completely calibrationless BCIs.

The remainder of this paper is organized as follows: Section II introduces two popular Euclidean space spatial filters, CSP and xDAWN. Section III introduces the RA-MDRM approach in the Riemannian space. Section IV proposes our Euclidean space data alignment approach. Section V compares the performances of our approach with RA-MDRM on two MI datasets and one ERP dataset. Finally, Section VI draws conclusions and points out several future research directions.

II. SPATIAL FILTERING IN THE EUCLIDEAN SPACE

Two popular spatial filters of EEG signals, CSP [12], [14], [17], [21] and xDAWN [22], [28], are introduced in this section. They will be used in the experiments in Section V.

A. Common Spatial Pattern (CSP)

CSP is a Euclidean space spatial filtering approach, particularly popular in MI based BCIs. Since the main task of MI is comparing the power of μ -rhythm from different

cortical areas, and the power is equivalent to the variance of the bandpassed EEG signals, CSP aims at projecting the bandpassed EEG signals into subcomponents which have the maximum difference in variance between two classes.

Let $X_i \in \mathbb{R}^{C \times T}$ be a bandpassed EEG trial, where C is the number of channels and T the number of time samples. Assume there are two classes (0 and 1), and the trials are $X_{0,i}$ ($i = 1, \dots, n_0$) and $X_{1,i}$ ($i = 1, \dots, n_1$), respectively. Then we compute the mean covariance matrix of the trials in Class c by:

$$\bar{\Sigma}_c = \frac{1}{n_c} \sum_{i=1}^{n_c} X_{c,i} X_{c,i}^T, \quad c = 0, 1 \quad (1)$$

Formally, CSP filters are obtained by:

$$W_0 = \arg \max_W \frac{\text{tr}(W^T \bar{\Sigma}_0 W)}{\text{tr}(W^T \bar{\Sigma}_1 W)}, \quad (2)$$

where $W_0 \in \mathbb{R}^{C \times F}$ is a filter matrix whose columns are the individual filters, and $\text{tr}(\cdot)$ is the trace of a matrix.

W_0 maximizes the variance for Class 0 while minimizing it for Class 1. In practice, we often construct a CSP filter matrix $W_* = [W_0, W_1] \in \mathbb{R}^{C \times 2F}$, where

$$W_1 = \arg \max_W \frac{\text{tr}(W^T \bar{\Sigma}_1 W)}{\text{tr}(W^T \bar{\Sigma}_0 W)}, \quad (3)$$

i.e., W_1 maximizes the variance for Class 1 while minimizing it for Class 0.

W_0 and W_1 are the concatenations of the F eigenvectors associated with the F largest eigenvalues of $\bar{\Sigma}_1^{-1} \bar{\Sigma}_0$ and $\bar{\Sigma}_0^{-1} \bar{\Sigma}_1$, respectively. Since $\bar{\Sigma}_1^{-1} \bar{\Sigma}_0$ and $\bar{\Sigma}_0^{-1} \bar{\Sigma}_1$ have the same eigenvectors, and their corresponding eigenvalues are reciprocal, W_* is the concatenation of the $2F$ eigenvectors associated with the F largest and F smallest eigenvalues of the matrix $\bar{\Sigma}_1^{-1} \bar{\Sigma}_0$ (or $\bar{\Sigma}_0^{-1} \bar{\Sigma}_1$), i.e., only one eigen decomposition is needed in computing W_* .

Once W_* is obtained, CSP projects an EEG trial $X \in \mathbb{R}^{C \times T}$ to $X' \in \mathbb{R}^{2F \times T}$ by:

$$X' = W_*^T X \quad (4)$$

Usually $2F < C$, so CSP can increase the signal-to-noise ratio and reduce the dimensionality simultaneously.

After CSP filtering, the logarithmic variance feature vector can be extracted by [8]:

$$\mathbf{x} = \log \left(\frac{\text{diag}(X' X'^T)}{\text{tr}(X' X'^T)} \right) \quad (5)$$

where $\text{diag}(\cdot)$ returns the diagonal elements of a matrix. These features were used in the LDA classifier in Section V.

B. xDAWN

The xDAWN algorithm [22], [28] is a popular spatial filtering approach for ERP-based BCIs. As mentioned in the Introduction, the neural mechanisms of MI and ERP are different. Compared with MI, the most useful information for ERP classification is in the time domain rather than the spatial domain. xDAWN first estimates the evoked P300 potentials,

and then uses these responses to build spatial filters to enhance the P300 signals.

Let X denotes a long course of EEG signals. Assume that:

$$X = PD^T + N, \quad (6)$$

where P is the time course of the P300 response, N represents the ongoing background brain activities as well as artifacts and noise, and D is a Toeplitz matrix whose first column is defined as:

$$D_{\tau_k,1} = \begin{cases} 1, & \tau_k \text{ is the onset of the } k\text{th target stimulus} \\ 0, & \text{otherwise} \end{cases} \quad (7)$$

Formally, xDAWN finds spatial filters $W_* \in \mathbb{R}^{C \times F}$ that maximize the signal to signal-plus-noise ratio:

$$W_* = \arg \max_W \frac{\text{tr}(W^T P D^T D P^T W)}{\text{tr}(W^T X X^T W)}, \quad (8)$$

The columns of W_* are the individual filters. They are the concatenation of the F eigenvectors associated with the F largest eigenvalues of $(X X^T)^{-1} P D^T D P^T$.

Similar to the CSP, xDAWN projects an EEG trial X from the original channel space to a new (usually much smaller) space by:

$$X' = W_*^T X. \quad (9)$$

Then feature extraction and machine learning can be performed on X' .

III. RA-MDRM

The covariance matrices of EEG trials are SPD, and lie in a Riemannian space instead of a Euclidean space [32]. Since the covariance matrices directly encode the spatial information of the EEG trials, and by appropriately augmenting the EEG trials (such as in ERP classification) they can also encode the temporal information, we can perform EEG classification directly based on the covariance matrices.

This section introduces the MDRM classifier, which assigns a trial to the class whose mean is the closest to its covariance matrix, and also a Riemannian space covariance matrix alignment approach (RA).

A. Riemannian Distance

The Riemannian distance between two points P_1 and P_2 is called the *geodesic*, which is given by the minimum length of a curve connecting them on the Riemannian manifold:

$$\delta_R(P_1, P_2) = \|\log(P_1^{-1} P_2)\|_F = \left[\sum_{r=1}^R \log^2 \lambda_r \right]^{\frac{1}{2}}, \quad (10)$$

where the subscript F denotes the Frobenius norm, and λ_r , $r = 1, 2, \dots, R$, are the real eigenvalues of $P_1^{-1} P_2$.

The Riemannian distance of two points P_1 and P_2 remains unchanged under linear invertible transformation:

$$\delta(C^T P_1 C, C^T P_2 C) = \delta_R(P_1, P_2) \quad (11)$$

where C is an invertible matrix. This property of the Riemannian distance is called *congruence invariance*.

B. Riemannian Mean

The mean of a set of SPD matrices can be computed in the Euclidean space as their arithmetic mean, and also be computed in the Riemannian space as the Riemannian mean (geometric mean), defined as the matrix minimizing the sum of the squared Riemannian distances:

$$\varrho(P_1, \dots, P_N) = \arg \min_P \sum_{n=1}^N \delta_R^2(P, P_n). \quad (12)$$

There is no closed-form solution for (12), and it is usually computed by an iterative gradient descent algorithm [10].

C. MDRM

The MDRM classifier [1], [7], [32] computes the covariance matrix of each EEG trial, and the Riemannian mean of each class using the labeled training trials, then assigns each test trial to the class whose Riemannian mean is the closest to its covariance matrix, i.e.,

$$g(\Sigma) = \arg \min_{c=1,2,\dots,C} \delta_R(\Sigma, \bar{\Sigma}^c), \quad (13)$$

where $\bar{\Sigma}^c$ is the Riemannian mean of Class c , Σ is the covariance matrix of the test trial, and $g(\Sigma)$ is the prediction of its class label.

D. RA-MDRM

Zanini et al. [33] proposed a novel TL approach in the Riemannian space, referred in this paper as RA-MDRM, to improve the performance of the MDRM classifier by utilizing auxiliary data from other sessions and/or subjects when there are only a few labeled trials from a new subject. Since the covariance matrices of the trials are the input to MDRM, RA-MDRM aims to align the covariance matrices from different sessions/subjects to make them more consistent. It is assumed that the change from one session/subject to another session/subject can be viewed as a geometric transformation of the covariance matrices, which can be simplified as a “shift” in the Riemannian space. This “shift” is induced by the difference in neural responses and electrode locations with respect to a reference state, and moves over the Riemannian manifold in the same direction when the subjects are performing the task. Thus, RA-MDRM estimates the reference state to capture the “shift” induced by the individual differences.

More specifically, RA-MDRM first computes the covariance matrices of some resting trials, $\{R_i\}_{i=1}^n$, in which the subject is not performing any task, and then computes the Riemannian mean of these matrices by

$$\tilde{R} = \arg \min_R \sum_{i=1}^n \delta_R^2(R, R_i), \quad (14)$$

\tilde{R} is the used as the reference matrix in RA-MDRM to reduce the inter-session/subject variability by the following transformation:

$$\tilde{\Sigma}_i = \tilde{R}^{-1/2} \Sigma_i \tilde{R}^{-1/2}, \quad (15)$$

where Σ_i is the covariance matrix of the i th trial, and $\tilde{\Sigma}_i$ is the corresponding aligned covariance matrix.

This transformation would not change the distance between the covariance matrices belonging to the same session/subject because of the congruence invariance property in (11), but makes the covariance matrices of different sessions/subjects move over the Riemannian manifold in different directions with respect to the corresponding reference matrices, and hence reduces the cross-session (-subject) differences. As a result, covariance matrices from different sessions/subjects can be aligned and become comparable if the reference states are appropriately estimated.

RA-MDRM can be applied to both MI and ERP data; however, there is an important difference in building covariance matrices in these two paradigms.

Specifically, the covariance matrix of an MI trial is simply computed as:

$$\Sigma_i = X_i X_i^T \quad (16)$$

Σ_i encodes the most discriminative information of MI signals, i.e., the spatial localization of the brain activity.

However, the main discriminative information of ERP trials is carried temporally rather than spatially. The normal covariance matrix such as (16) ignores this temporal information. So Barachant and Congedo [2] proposed a novel approach to augment the ERP trials so that their covariance matrices can also encode the temporal information. They first compute the mean of multiple P300 trials:

$$P_1 = \frac{1}{|I|} \sum_{i \in I} X_i, \quad (17)$$

where I is the index set of the P300 trials. They then build a super trial X_i^* by concatenating P_1 and X_i :

$$X_i^* = \begin{bmatrix} P_1 \\ X_i \end{bmatrix} \quad (18)$$

The covariances matrix of X_i^* can be decomposed into several blocks:

$$\Sigma_i^* = X_i^* (X_i^*)^T = \begin{bmatrix} \Sigma_{P_1} & C_{P_1, X_i}^T \\ C_{P_1, X_i} & \Sigma_{X_i} \end{bmatrix} \quad (19)$$

Σ_i^* contains not only spatial information from the original covariance matrix Σ_{X_i} , but also temporal information in the cross-covariance C_{P_1, X_i} .

In MI, the resting state is the time window that the subject is not performing any task, e.g., the transition window between two imageries. In ERP, particularly the RSVP, the stimuli are presented quickly one after another and the responses overlap, so it is difficult to find the resting state. [33] used the non-target stimuli as the resting state in ERP, which requires that some calibration trials from the new subjects must be known. That is, in ERP,

$$\tilde{R} = \arg \min_R \sum_{i \in I} \delta_R^2(R, \Sigma_i), \quad (20)$$

where I is the index set of the non-target trials, and Σ_i is the corresponding covariance matrix.

IV. EEG DATA ALIGNMENT IN THE EUCLIDEAN SPACE (EA)

Although RA-MDRM has demonstrated promising performance in several BCI applications [33], it still has some limitations:

- 1) RA-MDRM can only be used in the Riemannian space, whereas most signal processing and machine learning algorithms are proposed in the Euclidean space.
- 2) RA-MDRM uses the Riemannian mean of the covariance matrices, which is time-consuming to compute, especially when the number of EEG channels is large.
- 3) RA-MDRM for ERP classification needs some labeled non-target trials from the new subject to build the reference matrix, so it cannot completely eliminate the calibration.

To cope with these limitations, we propose an Euclidean space EEG data alignment approach (EA) that does not need any labeled data from the new subject, and can be computed much more efficiently.

Similar to the RA-MDRM, our approach is also based on a reference matrix \tilde{R} ,

$$\tilde{R} = \frac{1}{n} \sum_{i=1}^n X_i X_i^T \quad (21)$$

i.e., \tilde{R} is the arithmetic mean of the covariance matrices of all trials. We then perform the alignment by

$$\tilde{X}_i = \tilde{R}^{-1/2} X_i. \quad (22)$$

Note that (22) is inspired from (15), both of which ensure the Riemannian distances among the covariance matrices are kept unchanged after the alignment. However, (15) aligns the covariance matrices in the Riemannian space, whereas (22) aligns the raw EEG trials in the Euclidean space.

Compared with RA, EA has several desirable properties:

- 1) The aligned EEG trials lie in the Euclidean space, which can be used by any Euclidean space signal processing and machine learning approach. There are much more such approaches in the Euclidean space than in the Riemannian space, i.e., EA offers much more freedom in further processing.
- 2) EA can be computed much faster than RA, because EA uses the arithmetic mean as the reference matrix, whereas RA uses the Riemannian mean as the reference matrix.
- 3) EA does not need any label information from the new subject, whereas RA needs some label information for ERP applications.

V. EXPERIMENTS

This section compares our EA alignment approach with RA-MDRM for both MI and ERP classification. In each experiment there were multiple subjects, and each subject was first aligned independently, either in the Riemannian space using (15) or the Euclidean space using (22). We then used leave-one-subject-out cross-validation to evaluate the calibrationless classification performance: each time we picked one subject as the new subject (test set), and combined the EEG trials from all remaining subjects as the training set to build the classifier.

A. MI Datasets

Two open MI datasets from BCI Competition IV¹ were used. Their experimental paradigms were similar: In each session a subject sat in a comfortable chair in front of a computer. At the beginning of a trial, a fixation cross appeared on the black screen to prompt the subject to be prepared. A moment later, an arrow pointing to a certain direction was presented as a visual cue for a few seconds. In this period the subject was asked to perform a specific MI task without feedback according to the direction of the arrow. Then the visual cue disappeared from the screen and a short break followed until the next trial began.

The first dataset² (Dataset 1 [5]) was recorded from seven healthy subjects. For each subject two classes of MI were selected from three classes: left hand, right hand, and foot. Continuous 59-channel EEG signals were acquired for three sessions: calibration, evaluation, and special feature. Here we only used the calibration session data which provided complete marker information. Each subject had 100 trials from each class in the calibration session.

The second MI dataset (Dataset 2a³) consisted of EEG data from nine subjects. Each subject was instructed to perform four different MI tasks, namely the imagination of the movement of the left hand, right hand, both feet, and tongue. 22-channel EEG signals and 3-channel EOG signals were recorded at 250Hz. A training session and an evaluation session were recorded on different days for each subject. Here we only used the EEG data from the calibration session, which included complete marker information. Additionally, two classes (left hand and right hand) of motor imagery were selected and each class had 72 trials.

The EEG signals from both datasets were preprocessed using the Matlab EEGLAB toolbox [9], following the guideline in [4]. First, a band-pass filter (8-30 Hz) was applied to remove muscle artifacts, line-noise contamination and DC drift. Next, we extracted EEG signals between [0.5, 3.5] seconds after the cue appearance for Dataset 1, and [0.5, 2.5] for Dataset 2a, as our trials. Then EEG signals between [4, 5] seconds after the cue appearance were extracted as resting states for Dataset 1 and EEG signals between [4, 5.5] seconds after the cue appearance were extracted as resting states for Dataset 2a.

B. ERP Dataset

We used an RSVP dataset from PhysioNet [11]⁴ for ERP classification. It contained EEG data from 11 healthy subjects upon rapid presentation of images at 5, 6, and 10 Hz [16]. Each subject was seated in front of a computer showing a series of images rapidly. The images were aerial pictures of London falling into two categories, namely target images and non-target images. Target images contained a randomly rotated and positioned airplane that had been photo realistically superimposed, and non-target images did not contain airplanes. The task was to recognize if the images were target or non-target

from EEG signals, which were recorded from 8 channels at 2048 Hz.

For each presentation rate and subject there were two sessions represented by “a” and “b”, which indicated whether the first image was “target” or “non-target”, respectively. Here we used the 5 Hz version (five images per second) in session “a”. The number of samples for different subjects varying between 368 and 565, and the target to non-target ratio was around 1 : 9.

The continuous EEG data had been bandpass filtered between [0.15, 28] Hz. We downsampled the EEG signal from 2048Hz to 64Hz, and epoched each trial to the [0, 0.7] second interval time-locked to the stimulus onset.

C. Data Visualization

In order to visualize how EA reduces the individual differences, we use t-Stochastic Neighbor Embedding (t-SNE) [23], a nonlinear dimensionality reduction technique that embeds high-dimensional data for visualization in a two- or three-dimensional space, to show and compare the EEG trials before and after the alignment.

Each time we picked one subject as the test set, and combined the trials from the remaining subjects as the training set. The features fed into the classifier were represented as points in a two-dimensional space in each experiment. So, the visualization results are different when we pick a different subject as the test set. Fig. 1 shows the visualization of MI Dataset 1 for the first three subjects, each row corresponding to a different subject as the test subject. The red dots are trials from the test subject, and the blue dots are trials from the training subjects. In each row, the left plot shows the trials before alignment, and the right shows the trials after alignment. Corresponding visualization results for the first three subjects in MI Dataset 2a are shown in Fig. 3, and the RSVP dataset in Fig. 3.

Generally we can observe that the training trials (blue dots) may be scattered far away from the test trials (red dots) before alignment, especially in Fig. 1. So, applying a classifier designed on the training trials directly to the test trials may not achieve good performance. However, after the alignment, the training and test trials overlap with each other, i.e., the discrepancies between the training and test trials were significantly reduced.

D. Classification Performances on the MI Datasets

We first tested our EA approach on the two MI datasets, and compared their performances with RA-MDRM. In the Euclidean space, after the EA, we used CSP for spatial filtering and LDA for classification. More specifically, the following four approaches were compared:

- 1) MDRM: The basic MDRM classifier, as introduced in Section III-C. It does not include any data alignment.
- 2) RA-MDRM: It is the approach introduced in Section III-D, which aligns the covariance matrices first in the Riemannian space, and then performs MDRM.
- 3) CSP-LDA: It is a standard Euclidean space classification approach for MI, which spatially filters the EEG trials

¹<http://www.bbc.de/competition/iv/>.

²http://www.bbc.de/competition/iv/desc_1.html.

³http://www.bbc.de/competition/iv/desc_2a.pdf.

⁴<https://www.physionet.org/physiobank/database/ltrsvp/>.

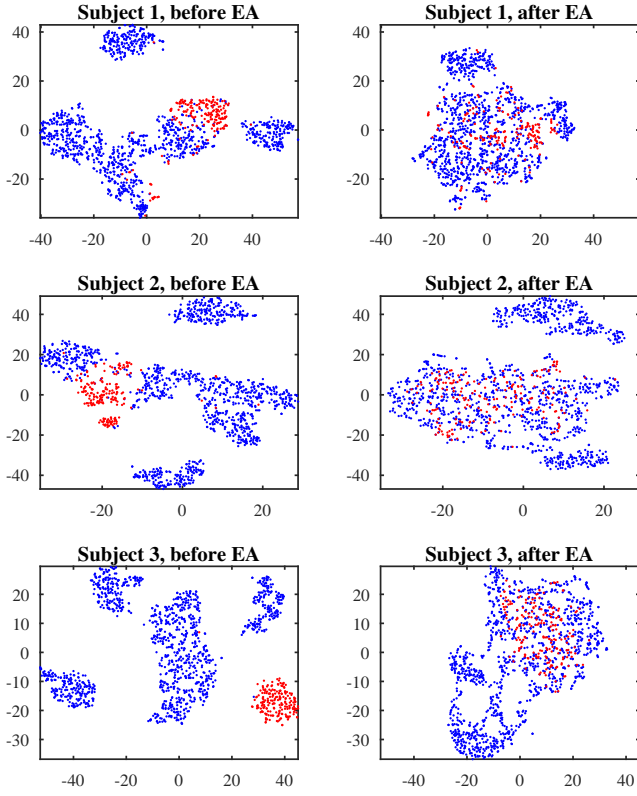


Fig. 1. Visualization of MI Dataset 1 for the first three subjects. Red dots: trials from the test subject; blue dots: trials from the training subjects; left plots: trials before alignment; right plots: trials after alignment.

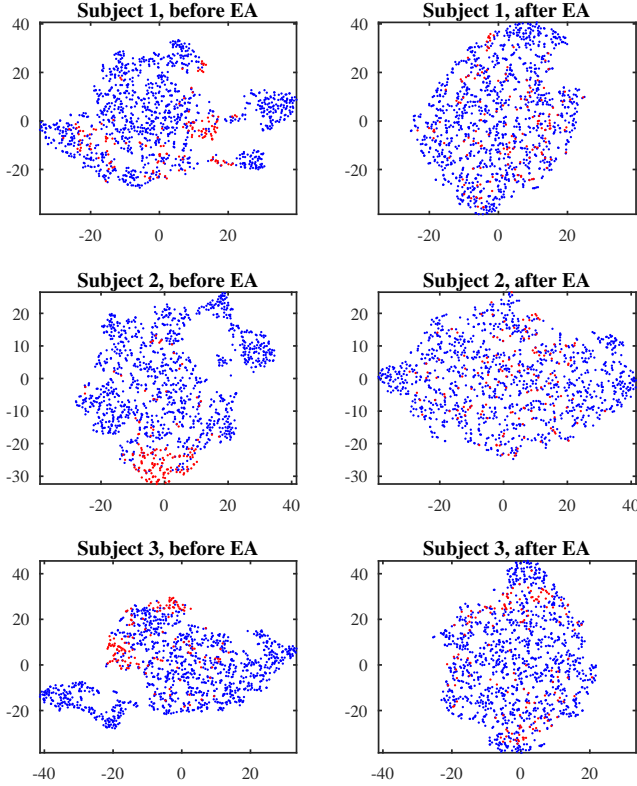


Fig. 2. Visualization of MI Dataset 2a for the first three subjects. Red dots: trials from the test subject; blue dots: trials from the training subjects; left plots: trials before alignment; right plots: trials after alignment.

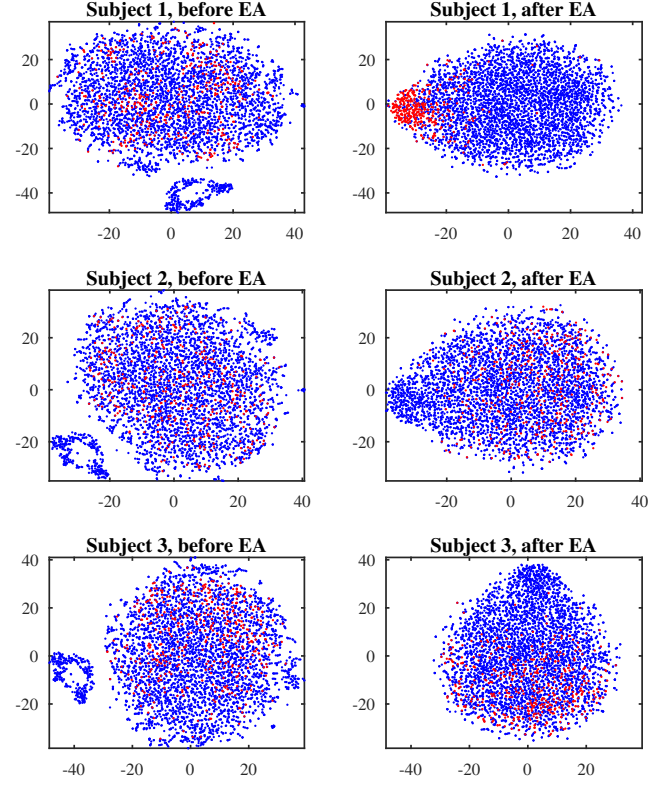


Fig. 3. Visualization of the RSVP Dataset for the first three subjects. Red dots: trials from the test subject; blue dots: trials from the training subjects; left plots: trials before alignment; right plots: trials after alignment.

by CSP and then classifies them by LDA, as introduced in Section II-A. It does not include any data alignment.

- 4) EA-CSP-LDA: It first aligns the EEG trials in the Euclidean space by our proposed EA approach (Section IV), and then performs CSP filtering and LDA classification.

The classification accuracies of the four approaches are shown in Fig. 4 and Table I. Observe that:

- 1) RA-MDRM outperformed MDRM on 15 out of the 16 subjects, suggesting that the Riemannian space covariance matrix alignment approach is effective.
- 2) EA-CSP-LDA outperformed CSP-LDA on all 16 subjects, suggesting that the proposed Euclidean space EEG trial alignment approach is also effective.
- 3) EA-CSP-LDA outperformed RA-MDRM on all seven subjects in Dataset 1, and on six out of the nine subjects in Dataset 2a, suggesting that the proposed Euclidean space EEG trial alignment approach, which enables the use of a wide range of Euclidean space signal processing and machine learning approaches, can be more effective than the Riemannian space covariance matrix alignment approach.

Additionally, it is interesting to compare the computational cost of different alignment approaches. The platform was a Dell XPS15 laptop with Intel Core i7-6700HQ CPU@2.60GHz, 16GB memory, and 512 GB SSD, running 64-bit Windows 10 Education and Matlab 2017a. The results are shown in Table II. Observe that our proposed approach

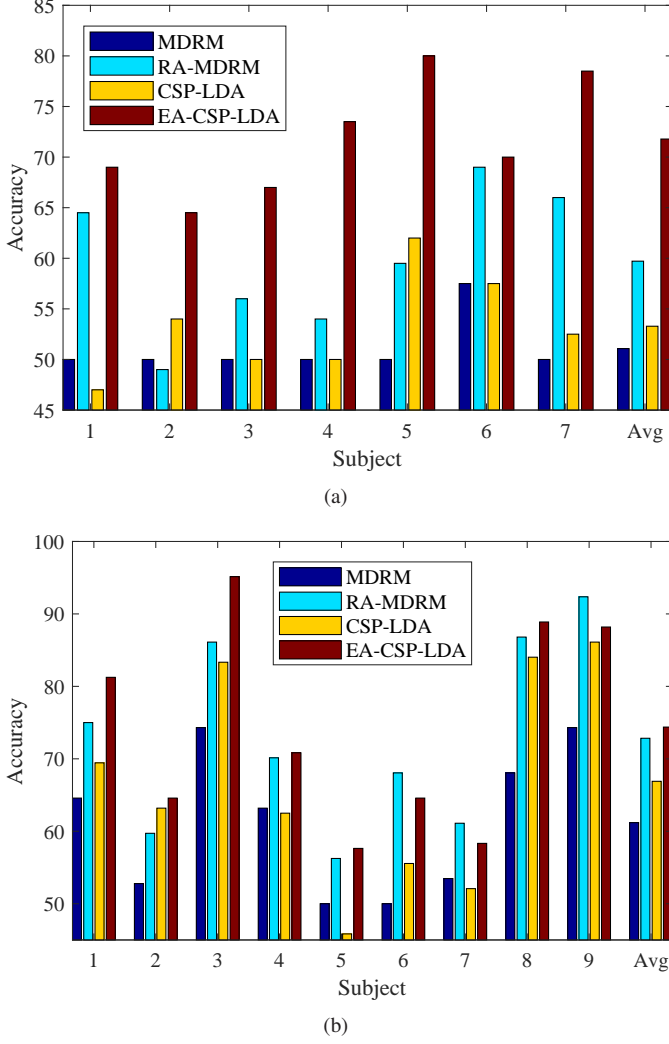


Fig. 4. Classification accuracies on the MI datasets: (a) Dataset 1; (b) Dataset 2a.

TABLE I
CLASSIFICATION ACCURACIES ON THE TWO MI DATASETS.

Dataset	Subject	MDRM	RA-MDRM	CSP-LDA	EA-CSP-LDA
1	1	50.0000	64.5000	47.0000	69.0000
	2	50.0000	49.0000	54.0000	64.5000
	3	50.0000	56.0000	50.0000	67.0000
	4	50.0000	54.0000	50.0000	73.5000
	5	50.0000	59.5000	62.0000	80.0000
	6	57.5000	69.0000	57.5000	70.0000
	7	50.0000	66.0000	52.5000	78.5000
	avg	51.0714	59.7143	53.2857	71.7857
2a	1	64.5833	75.0000	69.4444	81.2500
	2	52.7778	59.7222	63.1944	64.5833
	3	74.3056	86.1111	83.3333	95.1389
	4	63.1944	70.1389	62.5000	70.8333
	5	50.0000	56.2500	45.8333	57.6389
	6	50.0000	68.0556	55.5556	64.5833
	7	53.4722	61.1111	52.0833	58.3333
	8	68.0556	86.8056	84.0278	88.8889
	9	74.3056	92.3611	86.1111	88.1944
	avg	61.1883	72.8395	66.8981	74.3827

was 3.6-19.5 times faster than RA-MDRM, and also it had much smaller standard deviation.

TABLE II
THE COMPUTING TIME (SECONDS) OF EA-CSP-LDA AND RA-MDRM.

	EA-CSP-LDA		RA-MDRM	
	Mean	std	Mean	std
MI Dataset 1	0.3864	0.0514	7.5326	0.2200
MI Dataset 2a	0.2405	0.0322	0.8766	0.0729

In summary, we have demonstrated that our proposed Euclidean space EEG trial alignment approach is more effective and efficient than the Riemannian space covariance matrix alignment approach in MI classification.

E. Classification Performances on the RSVP Dataset

As RA-MDRM cannot be applied to ERP classification when there are no labelled trials at all for the new subject, we only validate the effectiveness of our EA approach by comparing it with the cases that no data alignment is used. More specifically, we compared the performances of the following four data preprocessing approaches (all trials have been bandpass filtered and downsampled to 64 Hz):

- 1) Principle component analysis (PCA), which performs PCA on the EEG trials to suppress noise and extract features. It does not include any data alignment.
- 2) EA-PCA, which performs EA first to align the trials from different subjects in the Euclidean space, and then performs PCA.
- 3) xDAWN-PCA, which performs xDAWN (Section II-B) first to spatially filter the EEG trials, and then performs PCA. It does not include any data alignment.
- 4) EA-xDAWN-PCA, which performs EA first to align the trials from different subjects in the Euclidean space, then xDAWN to spatially filter the EEG trials, and finally PCA.

In all approaches, the PCA extracted 20 features. The features were then normalized to $[0, 1]$ each, and libSVM [6] with a linear kernel was used for classification. The optimal parameter of the SVM was determined by cross-validation.

Because ERP-based BCIs usually have serious class imbalance problems, we used the balanced classification accuracy (BCA) to measure the performances. Let m^+ and m^- be the true number of trials from the target and non-target classes, respectively. Let n^+ and n^- be the number of trials that are correctly classified by an algorithm as target and non-target, respectively. Then, we first compute

$$a_+ = \frac{n^+}{m^+}, \quad a_- = \frac{n^-}{m^-}, \quad (23)$$

where a_+ is the classification accuracy on the target class, and a_- is the classification accuracy on the non-target class. The BCA is then computed as:

$$BCA = \frac{a_+ + a_-}{2}. \quad (24)$$

The BCAs for different approaches are shown in Fig. 5 and Table III. Observe that:

- 1) EA-PCA outperformed PCA on nine out of 11 subjects, suggesting that the proposed EA approach is effective for ERP classification.
- 2) EA-xDAWN-PCA outperformed xDAWN-PCA on eight out of 11 subjects, suggesting again that the proposed EA approach is effective for ERP classification.
- 3) On average xDAWN-PCA and PCA achieved similar performances, but EA-xDAWN-PCA achieved slightly better performance than EA-PCA, suggesting that our proposed EA may also help unleash the full potential of xDAWN.

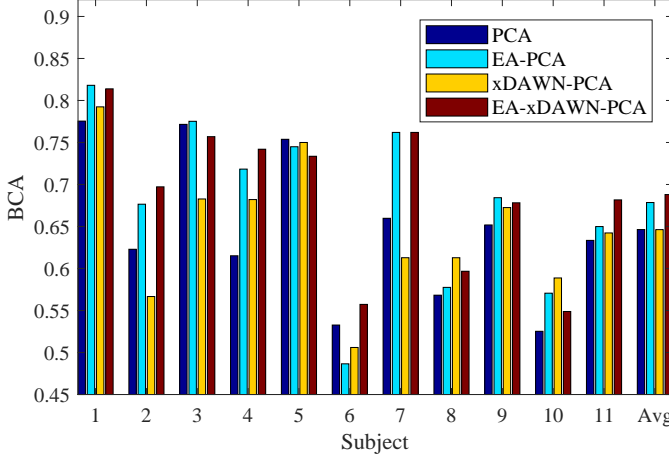


Fig. 5. BCAs on the RSVP dataset.

TABLE III
BCAs ON THE RSVP DATASET.

Subject	PCA	EA-PCA	xDAWN-PCA	EA-xDAWN-PCA
1	77.5445	81.8049	79.2408	81.3870
2	62.2882	67.6526	56.6652	69.7218
3	77.1559	77.5210	68.2753	75.6953
4	61.5170	71.8306	68.2058	74.1983
5	75.3788	74.4949	75.0000	73.3586
6	53.2692	48.6538	50.5983	55.7265
7	65.9753	76.1983	61.2844	76.1983
8	56.8242	57.7520	61.2827	59.6716
9	65.1835	68.4287	67.2532	67.8214
10	52.5242	57.0604	58.8724	54.8818
11	63.3459	64.9920	64.2316	68.1676
avg	64.6370	67.8536	64.6282	68.8026

F. Discussion: Different Choices of the Reference Matrix

Reference matrix estimation has a direct impact on the performance of the alignment algorithm. Specifically, RA uses the Riemannian mean of the resting covariance matrices for MI classification and the Riemannian mean of the non-target covariance matrices for ERP classification, as in (14) and (20), respectively. EA estimates the reference matrix from all trials by (21), whose procedure is the same for both MI and ERP classifications.

In summary, the reference matrix can be estimated from two types of trials for MI classification: 1) the *resting* trials that the subject is not performing any task; and, 2) the *imagery* trials that the subject is performing any motor imagery task.

Furthermore, the reference matrix can be computed as the Riemannian mean or the Euclidean mean. So we have four potential combinations: *Riemannian* mean of the *resting* trials (RR), *Euclidean* mean of the *resting* trials (ER), *Riemannian* mean of all *imagery* trials (RI), and *Euclidean* mean of all *imagery* trials (EI).

This subsection compares the performances of the above four reference matrices. The results are shown in Figs. 6(a) and 6(b) for MI Datasets 1 and 2a, respectively. For MDRM, using the Riemannian mean achieved better performance than using the Euclidean mean on both datasets. On the contrary, for CSP-LDA, using the Euclidean mean achieved better performance than using the Riemannian mean. This is consistent with our expectation: MDRM operates in the Riemannian space, and hence alignment in the Riemannian space sounds more reasonable; on the other hand, CSP-LDA operates in the Euclidean space, so alignment in the Euclidean space is more intuitive.

Additionally, Fig. 6 shows that for MDRM, the best performance was obtained when the Riemannian mean of all MI trials was used as the reference matrix; for CSP-LDA, the best performance was obtained when the Euclidean mean of all MI trials was used as the reference matrix. These suggest that the mean of the MI trials may be more useful than the mean of the resting trials.

VI. CONCLUSIONS AND FUTURE RESEARCH DIRECTIONS

Transfer learning is a promising approach for reducing the calibration effort of EEG-based BCI systems. It uses labeled data from other subjects involved in similar tasks to facilitate the calibration for a new subject. However, due to individual differences, if the EEG trials from different subjects are not aligned properly, the discrepancies among them may result in negative transfer. A Riemannian space covariance matrix alignment approach has been proposed to transform the covariance matrices of EEG trials to make them more consistent. However, it has some limitations: 1) the resulting aligned covariance matrices still lie in the Riemannian space, so a Riemannian space classifier must be used, whereas there are very few such classifiers; 2) its computational cost is high; and, 3) it needs some subject-specific calibration data from the new subject for ERP-based BCIs.

This paper has proposed an Euclidean space EEG trial alignment approach, which has three desirable properties: 1) the aligned EEG trials lie in the Euclidean space, which can be used by any Euclidean space signal processing and machine learning approaches (there are much more such approaches in the Euclidean space than in the Riemannian space); 2) it can be computed several times faster than the Riemannian space alignment approach; and, 3) it does not need any labeled trials from the new subject. Experiments on two MI datasets and one RSVP dataset verified the effectiveness and efficiency of our proposed approach.

Our future research directions include:

- 1) *Predict the performance improvement after alignment.*
We can observe from the results in Section V that the performance improvement of both the Riemannian space

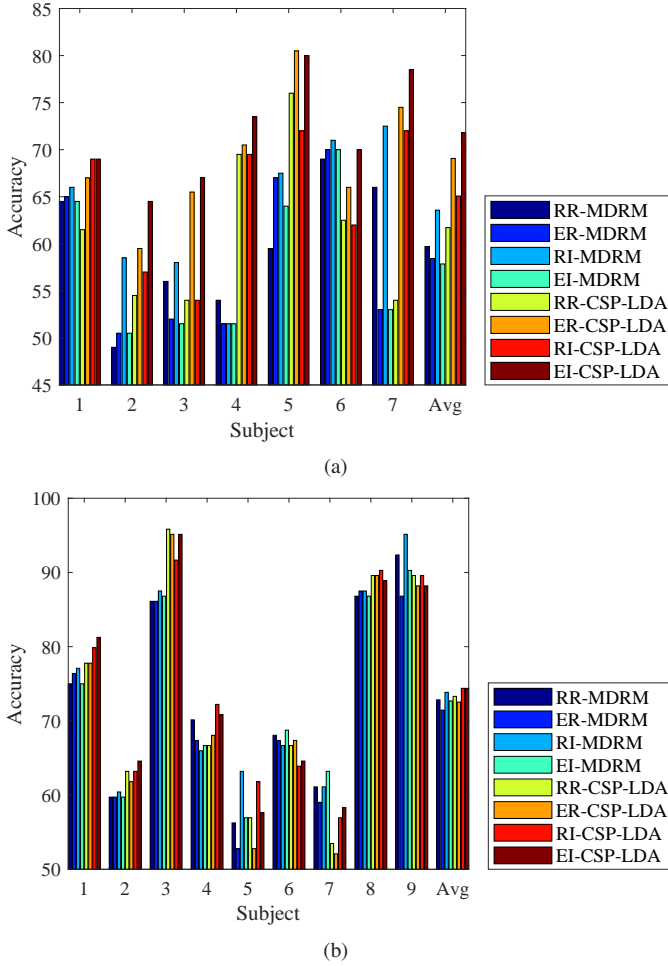


Fig. 6. Comparison of different reference matrices on the MI datasets. (a) Dataset 1; (b) Dataset 2a. RR: Riemannian mean of the resting trials; ER: Euclidean mean of the resting trials; RI: Riemannian mean of all imagery trials; EI: Euclidean mean of all imagery trials.

alignment and the Euclidean space alignment is more obvious when the discrepancies among the trials from different subjects are larger, e.g., Figs. 1-3 show that the discrepancies are the largest in MI Dataset 1, and the smallest in the RSVP dataset; as a result, the average performance improvements on MI Dataset 1 were the largest, and on the RSVP dataset were the smallest. It will be very useful to define a discrepancy measure so that we can predict how much performance improvement can be achieved after RA or EA.

- 2) *Make use of the label information of the training trials in EA.* All training trials contain label information, but this information is completely ignored in the EA. We conjecture that appropriately utilizing the labels could further benefit the alignment, as our final goal is classification, and considering the label information could make the trials more consistent at the per-class level, instead of now at the whole population level.
- 3) *Extend EA to supervised learning.* The current EA assumes the test trials are completely unlabeled, so it is an unsupervised approach. EA could be further improved if there are labeled trials from the new subject, as ex-

plained above. Additionally, when there are labeled trials from the new subject, more sophisticated TL approaches such as the weighted domain adaptation (wAR) [27], [29], [30] could be used to replace the LDA or SVM for further performance improvement.

REFERENCES

- [1] A. Barachant, S. Bonnet, M. Congedo, and C. Jutten, "Multiclass brain-computer interface classification by Riemannian geometry," *IEEE Trans. on Biomedical Engineering*, vol. 59, no. 4, pp. 920–928, 2012.
- [2] A. Barachant and M. Congedo, "A plug & play P300 BCI using information geometry," *arXiv: 1409.0107*, 2014.
- [3] C. M. Bishop, *Pattern Recognition and Machine Learning*. NY: Springer-Verlag, 2006.
- [4] B. Blankertz, R. Tomioka, S. Lemm, M. Kawanabe, and K. R. Muller, "Optimizing spatial filters for robust EEG single-trial analysis," *IEEE Signal Processing Magazine*, vol. 25, no. 1, pp. 41–56, 2008.
- [5] B. Blankertz, G. Dornhege, M. Krauledat, K. R. Muller, and G. Curio, "The non-invasive Berlin brain-computer interface: Fast acquisition of effective performance in untrained subjects," *NeuroImage*, vol. 37, no. 2, pp. 539–550, 2007.
- [6] C.-C. Chang and C.-J. Lin, "LIBSVM: A library for support vector machines," *ACM Trans. on Intelligent Systems and Technology*, vol. 2, no. 3, pp. 27:1–27:27, 2011.
- [7] M. Congedo, A. Barachant, and A. Andreev, "A new generation of brain-computer interface based on Riemannian geometry," *arXiv: 1310.8115*, 2013.
- [8] S. Dalhoumi, G. Dray, and J. Montmain, "Knowledge transfer for reducing calibration time in brain-computer interfacing," in *Proc. 26th IEEE Int'l Conf. on Tools with Artificial Intelligence*, Limassol, Cyprus, November 2014.
- [9] A. Delorme and S. Makeig, "EEGLAB: an open source toolbox for analysis of single-trial EEG dynamics including independent component analysis," *Journal of Neuroscience Methods*, vol. 134, pp. 9–21, 2004.
- [10] P. T. Fletcher and S. Joshi, "Principal geodesic analysis on symmetric spaces: Statistics of diffusion tensors," *Lecture Notes in Computer Science*, vol. 3117, pp. 87–98, 2004.
- [11] A. L. Goldberger, L. A. N. Amaral, L. Glass, J. M. Hausdorff, P. C. Ivanov, R. G. Mark, J. E. Mietus, G. B. Moody, C.-K. Peng, and H. E. Stanley, "PhysioBank, PhysioToolkit, and PhysioNet: Components of a new research resource for complex physiologic signals," *Circulation*, vol. 101, no. 23, pp. e215–e220, 2000.
- [12] H. He and D. Wu, "Transfer learning enhanced common spatial pattern filtering for brain computer interfaces (BCIs): Overview and a new approach," in *Proc. 24th Int'l. Conf. on Neural Information Processing*, Guangzhou, China, November 2017.
- [13] V. Jayaram, M. Alamgir, Y. Altun, B. Scholkopf, and M. Grosse-Wentrup, "Transfer learning in brain-computer interfaces," *IEEE Computational Intelligence Magazine*, vol. 11, no. 1, pp. 20–31, 2016.
- [14] Z. J. Koles, M. S. Lazar, and S. Z. Zhou, "Spatial patterns underlying population differences in the background EEG," *Brain Topography*, vol. 2, no. 4, pp. 275–284, 1990.
- [15] B. J. Lance, S. E. Kerick, A. J. Ries, K. S. Oie, and K. McDowell, "Brain-computer interface technologies in the coming decades," *Proc. of the IEEE*, vol. 100, no. 3, pp. 1585–1599, 2012.
- [16] A. Matran-Fernandez and R. Poli, "Towards the automated localisation of targets in rapid image-sifting by collaborative brain-computer interfaces," *PLoS ONE*, vol. 12, pp. 21–34, 2017.
- [17] J. Müller-Gerking, G. Pfurtscheller, and H. Flyvbjerg, "Designing optimal spatial filters for single-trial EEG classification in a movement task," *Clinical Neurophysiology*, vol. 110, no. 5, pp. 787–798, 1999.
- [18] L. F. Nicolas-Alonso and J. Gomez-Gil, "Brain computer interfaces, a review," *Sensors*, vol. 12, no. 2, pp. 1211–1279, 2012.
- [19] S. J. Pan and Q. Yang, "A survey on transfer learning," *IEEE Trans. on Knowledge and Data Engineering*, vol. 22, no. 10, pp. 1345–1359, 2010.
- [20] G. Pfurtscheller, G. R. Müller-Putz, R. Scherer, and C. Neuper, "Rehabilitation with brain-computer interface systems," *Computer*, vol. 41, no. 10, pp. 58–65, 2008.
- [21] H. Ramoser, J. Müller-Gerking, and G. Pfurtscheller, "Optimal spatial filtering of single trial EEG during imagined hand movement," *IEEE Trans. on Rehabilitation Engineering*, vol. 8, no. 4, pp. 441–446, 2000.

- [22] B. Rivet, A. Souloumiac, V. Attina, and G. Gibert, "xDAWN algorithm to enhance evoked potentials: application to brain-computer interface," *IEEE Trans. on Biomedical Engineering*, vol. 56, no. 8, pp. 2035–2043, 2009.
- [23] L. van der Maaten and G. Hinton, "Visualizing data using t-SNE," *Journal of Machine Learning Research*, vol. 9, pp. 2579–2605, 2008.
- [24] J. van Erp, F. Lotte, and M. Tangermann, "Brain-computer interfaces: Beyond medical applications," *Computer*, vol. 45, no. 4, pp. 26–34, 2012.
- [25] J. R. Wolpaw, N. Birbaumer, D. J. McFarland, G. Pfurtscheller, and T. M. Vaughan, "Brain-computer interfaces for communication and control," *Clinical Neurophysiology*, vol. 113, no. 6, pp. 767–791, 2002.
- [26] D. Wu, "Active semi-supervised transfer learning (ASTL) for offline BCI calibration," in *Proc. IEEE Int'l. Conf. on Systems, Man and Cybernetics*, Banff, Canada, October 2017.
- [27] D. Wu, "Online and offline domain adaptation for reducing BCI calibration effort," *IEEE Trans. on Human-Machine Systems*, vol. 47, no. 4, pp. 550–563, 2017.
- [28] D. Wu, J.-T. King, C.-H. Chuang, C.-T. Lin, and T.-P. Jung, "Spatial filtering for EEG-based regression problems in brain-computer interface (BCI)," *IEEE Trans. on Fuzzy Systems*, vol. 26, no. 2, pp. 771–781, 2018.
- [29] D. Wu, V. J. Lawhern, S. Gordon, B. J. Lance, and C.-T. Lin, "Driver drowsiness estimation from EEG signals using online weighted adaptation regularization for regression (OwARR)," *IEEE Trans. on Fuzzy Systems*, vol. 25, no. 6, pp. 1522–1535, 2017.
- [30] D. Wu, V. J. Lawhern, W. D. Hairston, and B. J. Lance, "Switching EEG headsets made easy: Reducing offline calibration effort using active weighted adaptation regularization," *IEEE Trans. on Neural Systems and Rehabilitation Engineering*, vol. 24, no. 11, pp. 1125–1137, 2016.
- [31] D. Wu, V. J. Lawhern, B. J. Lance, S. Gordon, T.-P. Jung, and C.-T. Lin, "EEG-based user reaction time estimation using Riemannian geometry features," *IEEE Trans. on Neural Systems and Rehabilitation Engineering*, vol. 25, no. 11, pp. 2157–2168, 2017.
- [32] F. Yger, M. Berar, and F. Lotte, "Riemannian approaches in brain-computer interfaces: a review," *IEEE Trans. on Neural Systems and Rehabilitation Engineering*, vol. 25, no. 10, pp. 1753–1762, 2017.
- [33] P. Zanini, M. Congedo, C. Jutten, S. Said, and Y. Berthoumieu, "Transfer learning: a Riemannian geometry framework with applications to brain-computer interfaces," *IEEE Trans. on Biomedical Engineering*, vol. 65, no. 5, pp. 1107–1116, 2018.